JOURNAL OF MATERIALS SCIENCE 37 (2002) 2851 – 2856

Martensitic transformation of an aged/thermal-cycled $Ti_{30.5}Ni_{49.5}Zr_{10}Hf_{10}$ shape memory alloy

S. F. HSIEH*
Department of Mold and Die Engineering, National Kaohsiung University of Applied Science, Kaohsiung, Taiwan 807, Republic of China
E-mail: sfhsieh@cc.kuas.edu.tw

W. K. CHANG
Institute of Materials Science and Engineering, National Dong Hwa University, Hualien, Taiwan 974, Republic of China

$Ti_{30.5}Ni_{49.5}Zr_{10}Hf_{10}$ alloy undergoes a B2 $\leftrightarrow$ B19′ one stage martensitic transformation. Martensitic transformation temperatures decrease, but the hardness increases with increasing aging time, resulting from the effect of point defects/atoms rearrangement in B2 phase induced by aging at 450°C. Thermal cycling can also decrease the transformation temperatures while increasing the hardness of the alloy. The strengthening effects of aging and thermal cycling on the M_s (M^*) temperature of this alloy follows the expression $M_s = T_0 - K\Delta\sigma y$, in which K values are affected by different strengthening processes. Experimental results indicate that martensitic transformation temperatures of $Ti_{30.5}Ni_{49.5}Zr_{10}Hf_{10}$ alloy can be more effectively depressed by aging than by thermal cycling. The K value of this aged alloy is smaller than that of aged $Ti_{40.5}Ni_{49.5}Zr_{10}$ alloy due to the former having the higher aged temperature and the less lattice distortion.

1. Introduction

Near-equiatomic TiNi shape memory alloys (SMAs) are technologically important materials with their superior shape memory effect and superelastic properties. The application of these alloys has spread not only to engineering but also to medical and dental fields. However, they are limited to use at temperatures lower than 150°C because their starting temperatures of martensitic transformation, M_s, are usually lower than 100°C. High-temperature SMAs with an M_s temperature higher than 100°C have been exhaustively researched owing to their potential applications. Ternary TiNiX high-temperature SMAs, with X being precious metals Pd, Pt and Au, also have been developed [1–3]. However, the high cost of precious metals will limit the practical applications of these SMAs. For this reason, other low-costs TiNiX SMAs need to be investigated. Among them, the most significant candidates are TiNiZr and TiNiHf alloys with Zr and Hf being used to replace Ti in these alloys.

Mulder *et al*. [4] reported that the M_s temperatures above 120°C can be obtained in TiNiZr alloys with Zr content above 10 at.% and Ni content below 49.5 at.%. They also found that the decrease in transformation temperatures in the thermal-cycled $Ti_{31.5}Ni_{48.5}Zr_{20}$ alloy is affected by the $(Ti,Zr)_2Ni$ precipitates. Meanwhile, the authors [5] reported that the lattice parameters of martensitic phase B19′ by using the XRD, TEM and Riverted method [6] are dependent on the Zr content in $Ti_{50.5-X}Ni_{49.5}Zr_X$ SMAs with Zr content in the range of 1 to 20 at.% at room temperature. Three phases (Ti,Zr)Ni, $(Ti,Zr)_2Ni$ and the λ_1 phase are observed in Ti-rich $Ti_{53-X}Ni_{47}Zr_X$ alloys with the Zr content in the range of 5–20 at.% at room temperature [7]. Here, λ_1 phase is a TiNiZr ternary solid solution and the (Ti,Zr)Ni phase can exhibit the B2 $\leftrightarrow$ B19′ martensitic transformation with the M_s temperature in the range of 60°C–260°C [7].

The transformation behavior and shape memory characteristics of Ti-rich TiNi and TiNiZr SMAs have been reported under various thermomechanical treatments, such as thermal cycling, aging and cold rolling [8, 9]. However, Ti-rich TiNi binary alloys with Ti being partially replaced by Hf and Zr, are seldom reported to have their transformation behavior and shape memory characteristics affected by these treatments. In the present study, we aim to understand the general characteristics of an aged or thermal-cycled Ti-rich $Ti_{30.5}Ni_{49.5}Zr_{10}Hf_{10}$ quaternary SMA, included its transformation temperatures, microstructures and internal friction properties, etc. The strengthening effects

*Author to whom all correspondence should be addressed.

in these thermomechanical treated specimens will also be discussed.

2. Experimental procedure

The conventional tungsten arc melting technique was employed to prepare $Ti_{30.5}Ni_{49.5}Zr_{10}Hf_{10}$ (in at.%) alloy. Titanium (purity 99.7 wt%), nickel (purity 99.9 wt%), zirconium (purity 99.8 wt%) and hafnium (purity 99.2 wt%), totaling about 120 g, were melted and remelted at least six times in an argon atmosphere. A pure titanium button was used as a getter during the arc melting. The mass loss during melting was negligibly small. The as-melted buttons were homogenized at 950°C for 72 hrs and then quenched in water. The homogenized buttons were cut into several plates with a low speed diamond saw, and then annealed at 900°C for 1 hr and quenched in water. After the annealing treatment, two experimental procedures were conducted. First, some plates were sealed in evacuated quartz tubes and aged at 450°C for 1 hr to 240 hrs and then quenched in water. Second, several more plates were subjected to thermal cycling N times from 0°C to 400°C with $N = 1$–100 cycles. Specimens for electrical resistivity measurement (size: 50 mm × 1 mm × 1 mm), DSC measurement, dynamic mechanical analysis (DMA, size: 25 mm × 4 mm × 0.5 mm), hardness test, shape recovery test and microstructure observation were carefully cut from plates treated by the above procedures.

Martensitic transformation temperatures were measured by using a four-probe electrical resistivity. The temperature range for electrical resistivity test was from 25°C to 450°C. DSC measurements was made with a Dupont 9990 thermal analyzer equipped with a quantitative scanning system 910 DSC cell for controlled heating and cooling runs on samples encapsulated in an aluminum pan. The running temperature range was from 0°C to 400°C with a heating and cooling rate of 10°C/min. The DMA tests were studied in a three-point bending configuration using a Dupont Dynamic Mechanical Analyzer, DMA-983. The internal friction, $Q^{-1} = \tan\delta$, and storage E' modulus measurements were performed at frequency $f = 1$ Hz and oscillation strain amplitude about 0.8 mm. The running temperature range was from 100°C to 400°C with a heating and cooling rate of 5°C/min. It is worth noting that, during the internal friction measurements, the temperature was monitored by a thermocouple located in a close neighborhood of the specimen, but not just located on it, and therefore the temperatures measured by the DMA-983 system are slightly shifted along the temperature axis with respect to those determined precisely by DSC measurements.

Specimens for the hardness test were first mechanically polished and then subjected to measurement in a microvickers hardness tester with 500 g load at room temperature. For each specimen, the average hardness value was taken from at least five test readings. The microstructure observations were made by optical microscope (OM) and transmission electron microscope (TEM). The shape recovery measurement was performed as described earlier by Lin *et al.* [10]. TEM specimens were prepared by electropolishing at 0°C with an electrolyte consisting of 20% H_2SO_4 and 80% CH_3OH by volume. Selected area diffraction patterns (SADPs) and TEM images were carried out using a JOEL-100CXII microscope operated at 100 kV and equipped with a conventional double tilting stage.

3. Experimental results and discussion

3.1. The effects of aging and thermal cycling on Ti-rich $Ti_{30.5}Ni_{49.5}Zr_{10}Hf_{10}$ alloy

Fig. 1 shows the experimental results of electrical resistivity versus temperature for the annealed $Ti_{30.5}Ni_{49.5}Zr_{10}Hf_{10}$ alloy. The notation for the determination of martensitic transformation temperatures, M_s, M_f, A_s and A_f, in Fig. 1 follows the example established by Hwang *et al.* [11]. The transformation thermal hysteresis (A_f–M_s) is approximately 45°C for this alloy, which is larger than that of $Ti_{51}Ni_{49}$ alloy ($\Delta T = 41$°C) [8], but is smaller than that of $Ti_{40.5}Ni_{49.5}Zr_{10}$ alloy ($\Delta T = 75$°C) [12]. This feature indicates that the Hf and/or Zr atoms solid solution in Ti-rich TiNi alloys will result in a different chemical free energy between binary TiNi and TiNi-based SMAs.

Fig. 2a shows the TEM bright field image of martensite in annealed $Ti_{30.5}Ni_{49.5}Zr_{10}Hf_{10}$ alloy. Fig. 2b–d are SADPs of Fig. 2a with $[100]_M$, $[010]_M$ and $[11\bar{1}]_M$ zones, respectively. It is noted that the twinning structure of Fig. 2c is identified as $(001)_M$ compound twin which corresponds to twin plates observed in Fig. 2a. Similar microstructure is also observed in $Ti_{40.5}Ni_{49.5}Zr_{10}$ alloy [12]. Han *et al.* [13] found that the lattice parameters of martensite in the $Ti_{36.5}Ni_{48.5}Hf_{15}$ alloy is a monoclinic B19′ structure with $a = 0.293$ nm, $b = 0.411$ nm, $c = 0.473$ nm and $\beta = 100.4°$ and the substructures of the martensite are $(001)_M$ type I and [011] type II twinning structures. The SADPs of Fig. 2b–d coincide with the results of Han's *et al.* [13]. Therefore, the structure of martensite in the $Ti_{30.5}Ni_{49.5}Zr_{10}Hf_{10}$ alloy is still monoclinic.

The internal friction, $\tan\delta$, and storage modulus E' spectra of annealed $Ti_{30.5}Ni_{49.5}Zr_{10}Hf_{10}$ alloy taken from the DMA test are shown in Fig. 3. There is one

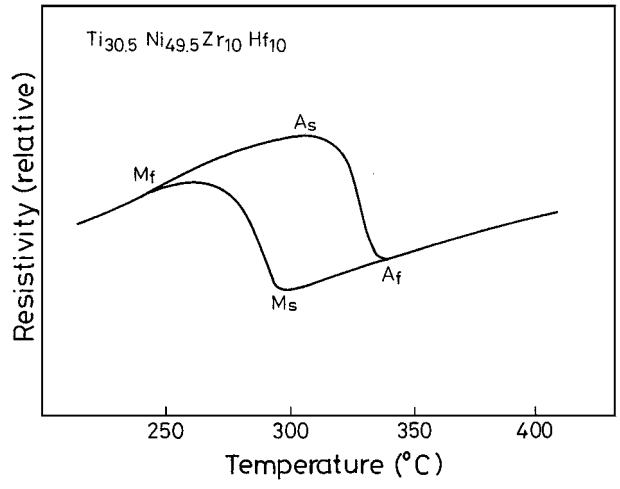

Figure 1 Electrical resistivity versus temperature curve for 900°C × 1 hr annealed and water quenched $Ti_{30.5}Ni_{49.5}Zr_{10}Hf_{10}$ alloy.

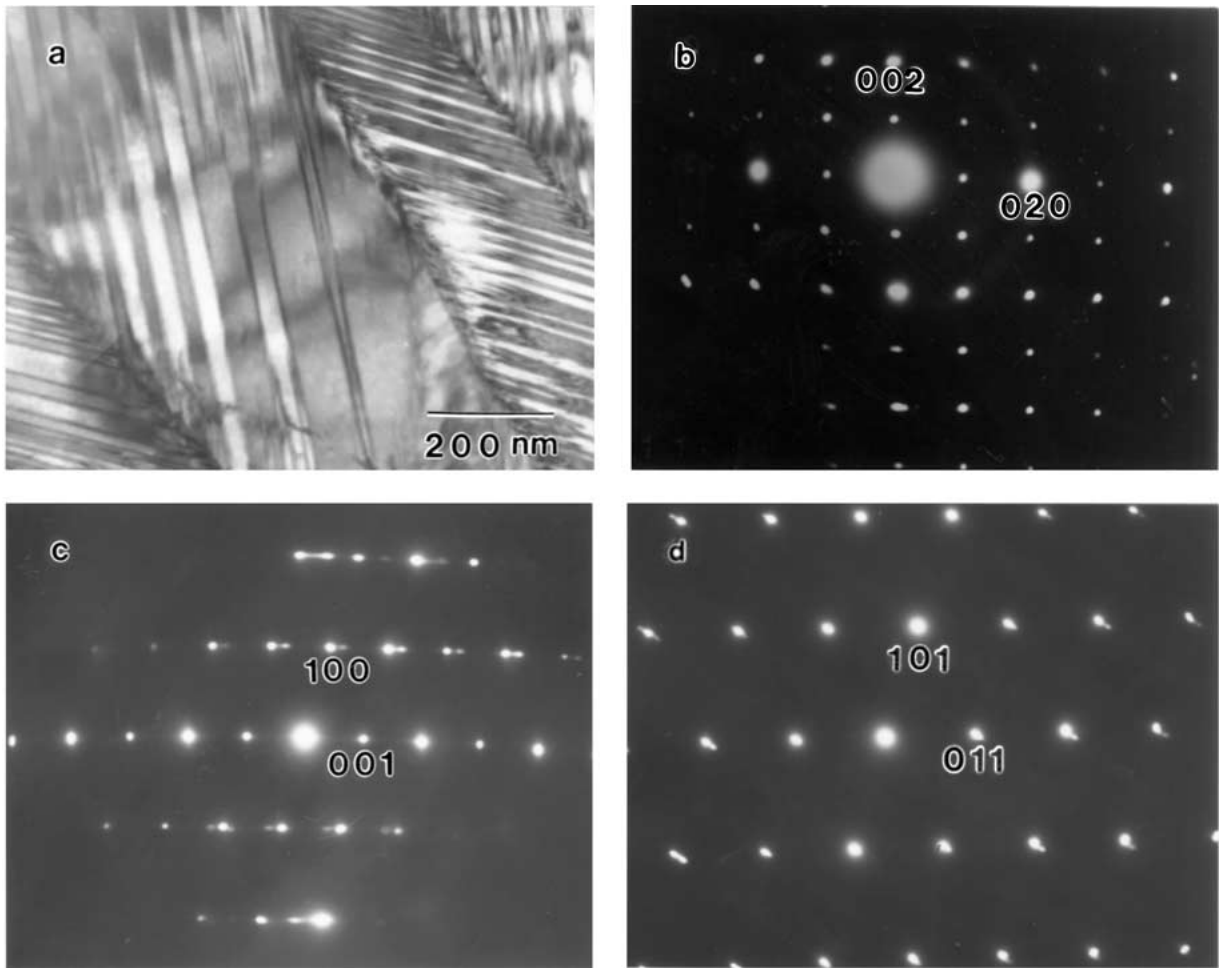

Figure 2 (a) Transmission electron micrographic bright-field image of as-annealed $Ti_{30.5}Ni_{49.5}Zr_{10}Hf_{10}$ alloy. (b) SADP of (a) with $[100]_M$ zone axis, (c) SADP of (a) with $[010]_M$ zone axis, (d) SADP of (a) with $[11\bar{1}]_M$.

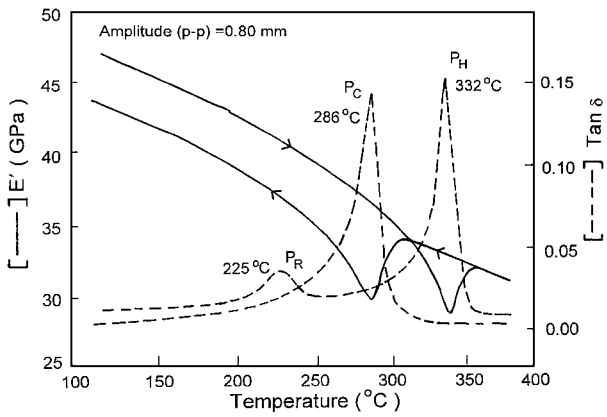

Figure 3 Evolution of elastic modulus and internal friction, $\tan\delta$, of $Ti_{30.5}Ni_{49.5}Zr_{10}Hf_{10}$ alloy on heating and cooling ($f = 1$ Hz, scanning rate = 5°C/min, oscillation strain amplitude = 0.80 mm). Peaks P_C and P_H are associated with the martensitic transformation and peak P_R is a relaxation one.

peak P_C at 286°C on cooling and one peak P_H at 332°C on heating and both peaks correspond to the minimum of modulus E'. Based on the electrical resistivity result of Fig. 1, the peak P_R appearing at 225°C in Fig. 3 not corresponding to the minimum of modulus E' is proposed to be a relaxation peak. The 240°C relaxation peak in TiNi binary alloy can be found in isothermal mechanical spectroscopy and is correspondent to a Zener relaxation [14]. The similar phenomena may be also occurred in $Ti_{30.5}Ni_{49.5}Zr_{10}Hf_{10}$ alloy. Besides, the relaxation peak is suggested to be associated with the interaction of dislocations and point defects [15] and is independent of the martensite and premartensite transformation [16]. As follows from Fig. 3, the storage modulus E' of martensite exhibits the non-linear behavior with a negative slope (i.e. it increases on cooling), but the similar case is for B2 parent phase in the temperature interval extending up to 380°C, which instead displays the linear increase on cooling, proving that a pronounced lattice softening occurs when approaching the M_s temperature. From Figs 1, 2 and 3, one can find that the transformation sequence of martensite in this alloy is the B2 $\leftrightarrow$ B19′ one-stage transformation.

Fig. 4 shows the same plot as Fig. 3, but now for the alloy aged at 450°C for 240 hrs. In Fig. 4, there is one peak, P_C, on cooling, and one peak, P_H, on heating in the first cycle. Peaks P_C and P_H are associated with the martensitic transformation. There is a well-shaped relaxation peak P_R appearing at 197°C, not corresponding to the minima of modulus E' in Fig. 4. The other plots of different aging time of this alloy are similar to plots of Fig. 3, except that the transformation temperature P_H, P_C and $\tan\delta$ are different, and are thus omitted here. P_H, P_C and P_R versus aging time of this alloy derived from the DMA test are plotted in Fig. 5. The hardness Hv versus aging time of this alloy

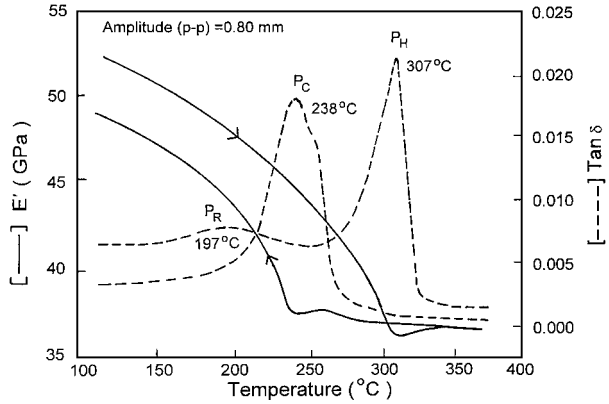

Figure 4 Evolution of elastic modulus and internal friction, $\tan\delta$, of $Ti_{30.5}Ni_{49.5}Zr_{10}Hf_{10}$ alloy aged at 450°C for 240 hrs on heating and cooling ($f = 1$ Hz, scanning rate = 5°C/min, oscillation strain amplitude = 0.80 mm). Peaks P_C and P_H are associated with the martensitic transformation and peak P_R is a relaxation one.

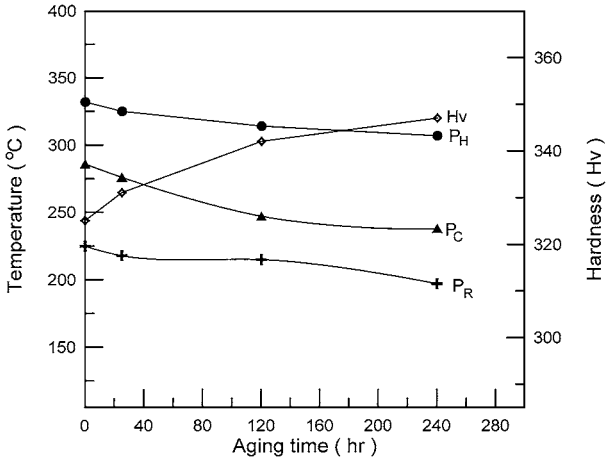

Figure 5 The peak temperatures of P_H, P_C, P_R and hardness versus aging time for $Ti_{30.5}Ni_{49.5}Zr_{10}Hf_{10}$ alloy aged at 450°C.

is also shown in Fig. 5. From Fig. 5, P_H, P_C and P_R in $Ti_{30.5}Ni_{49.5}Zr_{10}Hf_{10}$ alloy are all affected by aging time. The same characteristic shown in Fig. 5 also occurs in Ti-rich $Ti_{40.5}Ni_{49.5}Zr_{10}$ and $Ti_{51}Ni_{47}Si_2$ alloys [12, 17], but does not appear in $Ti_{51}Ni_{49}$ alloy [8].

Fig. 6a shows a TEM bright-field image of the B19′ martensite in a 450°C × 240 hr aged $Ti_{30.5}Ni_{49.5}Zr_{10}Hf_{10}$ alloy. Fig. 6b–c are SADPs of Fig. 6a, in which the foil are parallel to the $[100]_M$ and $[011]_M$ direction, respectively. Fig. 6c shows the micro-diffraction pattern taken from the martensite plate having fine striations at area *D* of Fig. 6a. No extra reflection spots can be observed in Fig. 6 except for the $(100)_M$ compound twins. Thus, the fine striations are traces of $(100)_M$ twin plates. Nishida *et al*. [18] reported that the $\{11\bar{1}\}$ type I, $\langle 011\rangle$ type II, $\{011\}$ type I, $(100)_M$ and $(001)_M$ compound twins in the B19′ martensite can be observed in TiNi binary alloy. Both the $(100)_M$ and $(001)_M$ compound twins have been recognized as a deformation twin [19, 20], since they do not give solution to the phenomenological crystallographic theory.

From Fig. 5, transformation temperatures of P_C and P_H decrease with increasing aging time. Since the precipitates have not been observed in aged

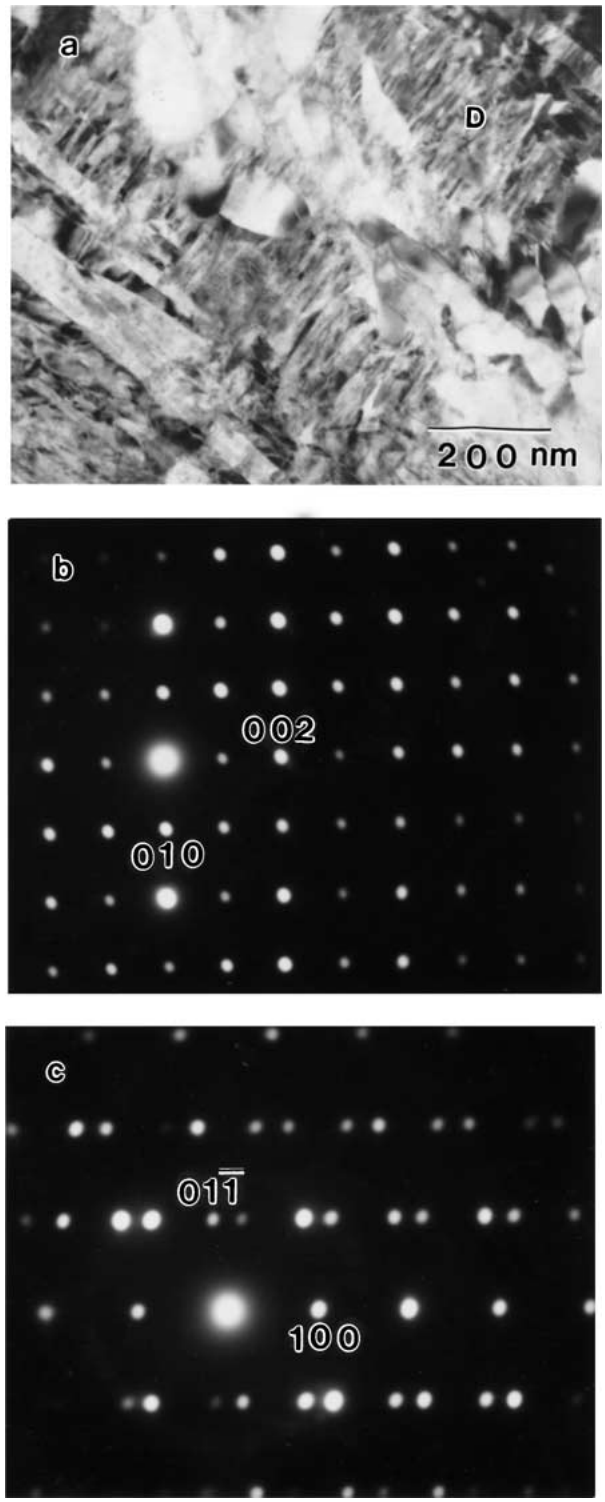

Figure 6 (a) Transmission electron micrographic bright-field image of $Ti_{30.5}Ni_{49.5}Zr_{10}Hf_{10}$ alloy aged at 450°C for 240 hrs. (b) SADP of (a) with $[100]_M$ zone axis (c) micro-diffraction pattern taken from area *D* in (a), showing $(100)_M$ compound twin with $[011]_M$ zone axis.

$Ti_{30.5}Ni_{49.5}Zr_{10}Hf_{10}$ alloy, compositional changes in the matrix can be ruled out. It has been reported that the shift of the transformation temperatures to lower values in aged $Ti_{32.3}Ni_{50}Hf_{17.7}$ [21] and $Ti_{40.5}Ni_{49.5}Zr_{10}$ [12] alloys are associated with the aging effects of point defects and atoms arrangement in B2 phase. Therefore, we propose that the excess quenched-in-vacancies can promote atomic rearrangement of Ti, Zr and Hf atoms in $Ti_{30.5}Ni_{49.5}Zr_{10}Hf_{10}$ alloy during the aging treatment at B2 phase. This rearranged process may

TABLE I DSC forward peak temperature, M^*, and hardness, Hv, for various thermal-cycled $Ti_{30.5}Ni_{49.5}Zr_{10}Hf_{10}$ alloy

Thermal cycles (N)	$Ti_{30.5}Ni_{49.5}Zr_{10}Hf_{10}$	
N	M^* (°C)	Hardness (Hv)
1	284	326
2	269	343
10	245	375
50	209	412
100	197	427

introduce microstrain field/lattice distortion and result in the hardness increment, as shown in Fig. 5. The lattice distortion will impede the mobility of twin plates in martensite and/or that of interfaces between the martensite and parent phase. At the same time, the intersitial atoms (such as H, O, etc.) can be put into solid solution in specimens during the arc melting process and the excess vacancies can be obtained by quenching the annealed specimen. Therefore, the interfaces between parent phase and martensite during martensitic transformation may be hindered by these point defects in aged specimens. The aged specimens have finer $(100)_M$ compound twins which have many defects such as dislocations, as shown in Fig. 6, most likely a result of the above mentioned aging effects.

Table I shows the DSC forward peak temperature M^* and the hardness Hv of the thermal-cycled $Ti_{30.5}Ni_{49.5}Zr_{10}Hf_{10}$ alloy. From Table I, the M^* temperature decreases, but the hardness Hv increases with increasing thermal cycling. It has been proposed that this feature comes from the influence of dislocations induced by thermal cycling in TiNi SMAs [22].

3.2. Strengthening effects in the aged and thermal cycled Ti-rich $Ti_{30.5}Ni_{49.5}Zr_{10}Hf_{10}$ alloy

Fig. 7 shows the relationship between peak temperature M^* and hardness Hv for the thermal-cycled and aged $Ti_{30.5}Ni_{49.5}Zr_{10}Hf_{10}$ alloy. The results of thermal-cycled $Ti_{51}Ni_{49}$ alloy and aged $Ti_{40.5}Ni_{49.5}Zr_{10}$ alloy are also plotted in Fig. 7. It was pointed out that any strengthening mechanism which impedes the transformation shear can lower the transformation temperatures because the martensitic transformation involves a shear process [23, 24]. This feature can be expressed by the Equation 1.

$$M_S = T_0 - K\Delta\sigma_y \quad (1)$$

The constant K contains the factors of proportionality between the critical shear stress and the yield stress $\Delta\sigma_y$, the equilibrium temperature T_0 is a function of the chemical composition, and the yield stress $\Delta\sigma_y$, is considered to be proportional to the hardness.

In this study, both thermal cycling and aging do not change the alloy's composition, hence T_0 is a constant. In addition, thermal cycling and aging can cause the alloy's hardness to increase, as shown in Fig. 5 and Table I. Therefore, both thermal cycling and aging can raise the yield stress $\Delta\sigma_y$. As derived from Equation 1, this feature should cause the M^* temperature to be lowered by the strengthening effect. This prediction is qualitatively consistent with the results of Fig. 7. A careful examination of Fig. 7 shows that the constant K of thermal-cycled $Ti_{30.5}Ni_{49.5}Zr_{10}Hf_{10}$ alloy is larger than that of thermal-cycled $Ti_{51}Ni_{49}$ alloy. We propose that the K value is related to the inherent hardness of annealed TiNi binary or TiNiXY quaternary alloys. The greater the annealed hardness, the larger the K value will be. For example, the thermal-cycled $Ti_{30.5}Ni_{49.5}Zr_{10}Hf_{10}$ alloy has an annealed hardness of 326 Hv and its K value is found to be 0.88°C/Hv, which is larger than that of thermal-cycled $Ti_{51}Ni_{49}$ (230 Hv, $K = 0.60$°C/Hv) alloy. In other words, the depression of M_s (M^*) temperature by the strengthening mechanism is stronger for the alloys having a higher annealed hardness.

The constant K of the thermal-cycled $Ti_{30.5}Ni_{49.5}Zr_{10}Hf_{10}$ alloy ($K = 0.88$°C/Hv) is smaller than that of the aged one ($K = 2.36$°C/Hv). This feature is a result of the different strengthening mechanism, because the former strengthening originates from the thermal cycled induced dislocations and the latter one results from the aging effects of point defects and atoms rearrangement in B2 phase. The fact that $K = 2.36$°C/Hv $> K = 0.88$°C/Hv also indicates that the martensitic transformation temperatures of $Ti_{30.5}Ni_{49.5}Zr_{10}Hf_{10}$ alloy can be more effectively depressed by aging in B2 phase than by B2 $\rightarrow$ B19′ thermal cycling. Meanwhile, the K value (2.36°C/Hv) of the aged $Ti_{30.5}Ni_{49.5}Zr_{10}Hf_{10}$ alloy is smaller than that of the aged $Ti_{40.5}Ni_{49.5}Zr_{10}$ alloy ($K = 3.08$°C/Hv) [12]. This phenomenon may be understood as follows: the higher the aged temperature, the less the lattice distortion will be. In this study, the specimens are all aged at 450°C in B2 phase. We can expect the aging effects of atoms rearrangement accompanied by a relaxation of internal stresses to reduce the lattice distortion in $Ti_{30.5}Ni_{49.5}Zr_{10}Hf_{10}$ alloy at 450°C to be more than that of $Ti_{40.5}Ni_{49.5}Zr_{10}$ alloy at 300°C.

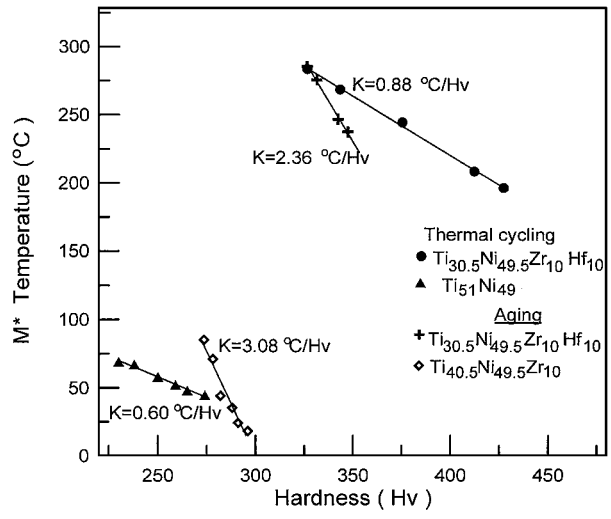

Figure 7 The M^* temperature versus hardness Hv for thermal cycled and aged $Ti_{30.5}Ni_{49.5}Zr_{10}Hf_{10}$ alloy. The data for the thermal-cycled $Ti_{51}Ni_{49}$ and aged $Ti_{40.5}Ni_{49.5}Zr_{10}$ alloys are also included.

Therefore, less driving force is needed to transform the Ti-rich $Ti_{30.5}Ni_{49.5}Zr_{10}Hf_{10}$ alloy. This account may explain why, for the same strengthening mechanism, $Ti_{30.5}Ni_{49.5}Zr_{10}Hf_{10}$ alloy has the lower K value observed in Fig. 7.

4. Conclusions

1. The annealed $Ti_{30.5}Ni_{49.5}Zr_{10}Hf_{10}$ alloy undergoes the one stage $B2 \leftrightarrow B19'$ martensitic transformation. Transformation temperatures decrease and hardness increases with increasing aging time at 450°C. This feature is related to the aging effects of point defects and atoms rearrangement in B2 phase. Besides, the finer plates formed in $(100)_M$ compound twins for the longer aged specimen may relate to these aging effects.

2. Transformation temperatures decrease and the hardness increases in the thermal-cycled $Ti_{30.5}Ni_{49.5}Zr_{10}Hf_{10}$ alloy. The strengthening effect of thermal cycling and aging on transformation temperatures of this alloy is found to be in accord with the equation $M_s = T_0 - K\Delta\sigma_y$. Experimental results show that K values are associated with the alloy's annealed hardness. The annealed hardness of $Ti_{30.5}Ni_{49.5}Zr_{10}Hf_{10}$ alloy is higher than that of $Ti_{51}Ni_{49}$ alloy owing to Zr and Hf atoms in solid solution in the TiNi alloy, and thus has a higher K value. Besides, the constant K of thermal-cycled $Ti_{30.5}Ni_{49.5}Zr_{10}Hf_{10}$ alloy ($K = 0.88$°C/Hv) is smaller than that of aged one ($K = 2.36$°C/Hv). This result indicates that martensitic transformation temperatures of $Ti_{30.5}Ni_{49.5}Zr_{10}Hf_{10}$ alloy can be more effectively depressed by aging in B2 phase than by $B2 \leftrightarrow B19'$ thermal cycling. The K value of aged $Ti_{30.5}Ni_{49.5}Zr_{10}Hf_{10}$ alloy is smaller than that of aged $Ti_{40.5}Ni_{49.5}Zr_{10}$ alloy ($K = 3.08$°C/Hv) due to the former having the higher aged temperature and the less lattice distortion.

Acknowledgement

The authors sincerely acknowledge the financial support of this study by the National Science Council (NSC), Republic of China, under Grants NSC 86-2216-E002-033 and NSC 89-2216-E151-010.

References

1. Y. C. LO, S. K. WU and C. M. WAYMAN, *Scripta Metall.* **24** (1990) 1571.
2. P. G. LINDQIST and C. M. WAYMAN, in "Engineering Aspects of Shape Memory Alloys," edited by T. W. Duering, K. N. Melton, D. Stockel and C. M. Wayman (Butterworth Heinemann, London, 1990) p. 58.
3. S. K. WU and C. M. WAYMAN, *Metallography* **20** (1987) 359.
4. J. H. MULDER, J. H. MASS and J. BEYER, in ICOMAT (1992) p. 869.
5. S. F. HSIEH and S. K. WU, *J. Alloys and Compounds* **270** (1998) 237.
6. H. M. RIETVELD, *J. Appl. Crystallogr.* **2** (1969) 65.
7. S. F. HSIEH and S. K. WU, *J. Alloys and Compounds* **266** (1998) 276.
8. H. C. LIN, S. K. WU and J. C. LIN, *Materials Chemistry and Physics* **37** (1994) 184.
9. S. F. HSIEH and S. K. WU, *J. Materials Characterization* **41** (1998) 151.
10. H. C. LIN and S. K. WU, *Scripta Metall.* **26** (1992) 59.
11. C. M. HWANG, M. MEICHLE, M. B. SALAMON and C. M. WAYMAN, *Phil. Mag.* A **47** (1983) 9.
12. S. K. WU and S. F. HSIEH, *J. Alloys and Compounds* **297** (2000) 294.
13. X. D. HAN, W. H. ZOU, R. WANG, Z. ZHANG and D. Z. YANG, *Acta Mater.* **44** (1996) 3711.
14. V. PELOSIN, F. DEBORDE and A. RIVIERE, *J. of De Physique, IV* **6** (1996) 93.
15. H. C. LIN, PhD. thesis, Institute of Materials Science and Engineering, National Taiwan University, Taipei, Taiwan, 1997.
16. J. S. ZHU, R. SCHALLER and W. BENOIT, *Phys. Lett.* A **141** (1989) 177.
17. S. F. HSIEH and S. K. WU, *J. Alloys and Compounds* **335** (2002) 254.
18. M. NISHIDA, K. YAMAUCHI, I. ITAI, H. OHGI and A. CHIBA, *Acta. Metall.* **43** (1995) 1229.
19. M. NISHIDA, H. OHGI, I. ITAI, A. CHIBA and K. YAMAUCHI, *ibid.* **43** (1995) 1219.
20. K. M. KNOWLES, *Phil. Mag.* A **45** (1982) 357.
21. R. SANTAMARTA, C. SEGUI, J. PONS and E. CESARI, *Scripta Materia.* **41** (1999) 867.
22. S. MIYAZAKI, T. IMAI, Y. IGO and K. OTSUKA, *Metall. Trans.* **17A** (1986) 76.
23. M. COHEN, E. S. MACHLIN and V. G. PARANJPE, in "Thermodynamics in Physical Metallurgy" (ASM, Metals Park, Ohio, 1950).
24. E. HORNBOGEN, *Acta Metall.* **33** (1991) 595.

Received 17 December 2001
and accepted 9 April 2002